LBL-13985

Conf-811231--3

Lawrence Berkeley Laboratory

UNIVERSITY OF CALIFORNIA

Physics, Computer Science & Mathematics Division

Presented at the Second Topical Forward Collider Physics Conference, Madison, WI, December 10-12, 1981

GLUON BREMSTRAHLUNG EFFECTS IN LARGE $p_\perp$ HADRON-HADRON SCATTERING

G.C. Fox and R.L. Kelly

February 1982

MASTER

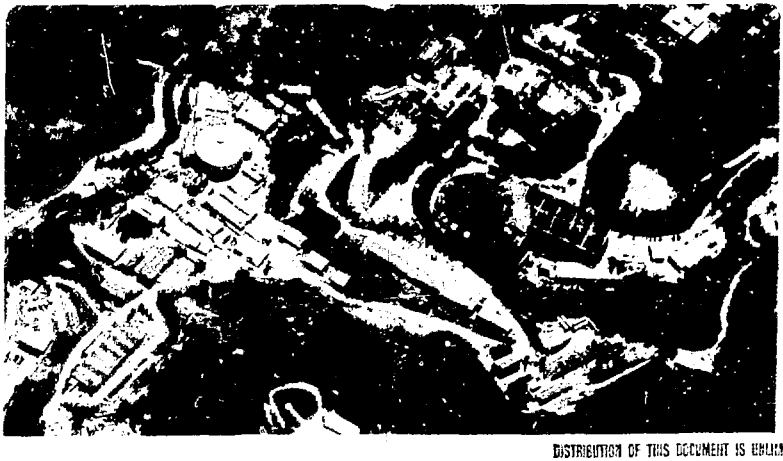

DISTRIBUTION OF THIS DOCUMENT IS UNLIMITED

Prepared for the U.S. Department of Energy under Contract W-7405-ENG-48

DISCLAIMER

LBL—13985
CALT-68-890

LBL--13985

DE82 008871

GLUON BREMSTRAHLUNG EFFECTS IN LARGE $p_\perp$ HADRON-HADRON SCATTERING

G. C. Fox
California Institute of Technology, Pasadena, CA. 91125

R. L. Kelly
Lawrence Berkeley Laboratory, University of California
Berkeley, CA 94720

ABSTRACT

We consider effects of parton (primarily gluon) *bremstrahlung* in the initial and final states of high transverse momentum hadron-hadron scattering. Monte Carlo calculations based on conventional QCD parton branching and scattering processes are presented. The calculations are carried only to the parton level in the final state. We apply the model to the Drell-Yan process and to high transverse momentum hadron-hadron scattering triggered with a large aperture calorimeter. We show that the latter triggers are biased in that they select events with unusually large bremstrahlung effects. We suggest that this trigger bias explains the large cross section and non-coplanar events observed in the NA5 experiment at the SPS.

INTRODUCTION

Leptoproduction and hadronic scattering in QCD are characterized by the non-scaling behavior of structure functions. This behavior arises from parton branching processes which alter the longitudinal momentum distribution of the hadronic constituents, typically increasing the structure functions at small x and decreasing them at large x. The mechanism for this is the radiation of partons (principally gluons) by the active partons in a hard scattering process. The radiated partons carry off longitudinal momentum and this increases the liklihood that the hard scattering occurs between partons at low x. In the familiar Altarelli-Parisi (1) approach one characterizes the hadronic initial state by Q^2-dependent structure functions for the active partons, and ignores the radiated partons. Furthermore the kinematics are usually simplified to neglect the Q^2- evolution of constituent transverse momentum. A fixed, x-independent constituent transverse momentum distribution is generally used for all values of Q^2. In this paper we use an approach in which each parton branching is governed by the basic Altarelli-Parisi kernels, but we also keep track of all the radiated partons and their subsequent branchings. We use full off-shell kinematics and follow the transverse momentum evolution of the active and radiated partons. We treat final states at the parton level only, and therefore consider large aperture experi-

This work was supported by the Division of High Energy Physics of the U.S. Department of Energy under Contract Nos. W-7405-ENG-48; and DE-AC03-81-ER40050.

ments which are less sensitive to hadronization effects than jet or single particle trigger experiments. We will see that even at the parton level, one can understand some of the main features of calorimeter experiments in terms of gluon radiation effects.

In the following section we describe the QCD evolution model used in our calculations. In Sec. III we describe trigger bias effects in large aperture calorimeters and give our results for the NA5 calorimeter. Sec. IV is a discussion of the Drell-Yan processes in our model, particularly our use of the Drell-Yan $p_\perp$ spectrum to choose the initial parton distributions. Details of the NA5 calculation, including $p_\perp^{hard}$ spectra and planarity distributions, are given in Sec. V, and in Sec. VI we give some predictions and comments concerning $\bar{p}p$ interactions at SPS collider energies.

II. THE MODEL

The model used was described in detail in Ref. (2) and essentially the same ideas have been used by Odorico in the talk presented at this conference (3). The methods were developed from the original ideas of Fox and Wolfrom (4) and Odorico and collaborators (5) for e^+e^- annihilation.

Hadron-hadron scattering in our formalism is illustrated in Figure 1 while some useful definitions are collected together in Tables 1&2. In the center of Figure 1, we see the conventional hard scattering in which the transverse momentum is $p_\perp^{hard}$. In the normal treatment (see for instance (6), one neglects the mass of the four partons involved in this collision (denoted by heavy lines in the figure). One further uses a phenomenological transverse momentum distribution for the initial state partons while the logitudinal momentum distributions $G(x,t_B^{min})$ are taken from leptoproduction experiments. The transverse momentum distribution for the partons is taken from measurements of the Drell-Yan process. This picture produces a four jet final state: two jets corresponding to the scattered partons and two correspond to the "beam remains" left after the initial state patrons are removed from the incident hadrons. Often one will try to make realistic predictions for the complete structure of these events by hadronizing the four jets usually employing the Field Feynman model (7). This does in fact provide a good first description of high $p_\perp$ events (6,8) although as we see from the NA5 data it does not describe large aperture calorimeter measurements! There are many things wrong with this calculation.

(1) As emphasized in ref. (9), the partons involved in the collision do not have zero mass but in fact must be off shell. The initial state partons have negative m^2 and those in the final state positive m^2.

(2) The four jet final state is only an approximation for (especially) gluon bremstrahlung from the initial and final partons produce multi-jet final states of complex topology.

(3) The transverse momentum distribution gets broader as one increases one's scale $|t_B^{min}|$ i.e. as one increases $p_\perp^{hard}$. This is already clear from the Drell-Yan data (of Section IV) but is not included in most calculations.

(4) Not only are there significant real emission processes mentioned in (2) but als virtual corrections are expected to be large [10].

(5) A convincing theoretical justification for the whole procedure - especially when it involves hadronization - is lacking [2]. Even if one is brave enough to use these methods, one cannot expect very precise results.

The techniques used in this paper put in the bremstrahlung from both the initial and final state partons and answer the first three objections above. The calculation employs the leading logarithm approximation and so is not exact but it does properly sum the bremstrahlung to all orders in α_s. We do not address the problems (4) and (5). However there is no reason to believe that the virtual corrections in (4) will alter the qualitative structure of the events and so if we concentrate on general features and not precise estimates, we should be quite safe. In fact we will only present results at the parton level here and so difficulties with hadronization are also avoided.

Returning to Figure 1, we see that the initial state partons start off with a mass^2 $t = t_B^o$ which we will take as -4 GeV^2. † These partons evolve toward the scale t_B^{min} emitting gluons (and quarks in the manner described in Ref. [2]. Note that the "beam remains" are no longer a simple jet and are further $Q^2(t_B^{min})$ dependent. The remains consist of the low-$p_\perp$ jet remaining after removal of the initial parton (as this parton is not far off shell, this part of the remains does have limited $p_\perp$) plus the Q^2 dependent collection of radiated partons. The effect of this radiation

†To be precise, one should in fact take the initial partons to have a mass^2 > t_B^o with a distribution $\alpha_s(t)/_t$.

increases with Q^2 and is reflected both in an increasing $p_\perp$ of the parton just before it scatters - we call this $p_\perp^{brem}$ (t_B^{min}) - and an increasing complexity of the remains. This $p_\perp^{brem}$ is what is often called the "intrinsic" transverse momentum of the partons inside the hadron. The above discussion makes it clear that this transverse momentum is scale dependent; on the other hand it is universal (at least in the leading logarithm approximation) and all processes governed by the same scale do exhibit the same transverse momentum distribution. Usually (6) one employs scale dependent logitudinal momentum distributions $G(x,Q^2)$ using analytic methods to sum the radiation effects. Our Monte Carlo reproduces (approximately) the same $G(x,Q^2)$ but has the important advantage of also estimating the associated Q^2 dependent effects in the beam remains and the $p_\perp^{brem}$ distribution.

In implementing our ideas we have to decide on the scale t_B^{min}. Unfortunately this decision is outside the leading logarithm approximation and no firm answer can be given. We remind the reader that this difficulty crops up in the conventional discussion of hadron-hadron scattering (6) in the choice of the argument Q^2 of $G(x,Q^2)$. We will in fact make not the best but the most convenient choice which in fact saves a large amount of computer time! The problem in applying our method to pp scattering is that one must choose t_B^{min} before starting the evolution and hence before knowing the four vectors of the final partons. Thus the only reasonable choice for the Drell-Yan process, i.e. $t_B^{min} \alpha - m^2_{\mu^+\mu^-}$, gives difficulties because one has the constraint that the c.m.s. energy^2, $\hat{s}$ of the scattered partons must match (at least approximately) the value of t_B^{min}. This rarely happens and so must generate many "wasted" events. In hadron-hadron scattering we avoid this difficulty by choosing a value $t_B^{min} = -4(p_\perp^{hard})^2$ which is essentially decoupled from $\hat{s}$. Any observed cross section σ is calculated as an integral

$$\sigma = \int dp_\perp^{hard} \frac{d\sigma^{constituent}}{dp_\perp^{hard}}$$

In Figure 2, we compare the new cross-section for this choice of t_B^{min} with that in ref. (6) for the NA5 energy. The two calculations have the same $p_\perp^{hard}$ shape but our new results are normalized a factor 1.5 below the old calculations. In fact the different Q^2 choice makes a factor of 3 difference but the exact kinematics used

in the new method restores a factor of 2. We feel that QCD calculations are currently uncertain to at least a factor of 2 and do not consider the difference in Figure 2 significant.

In Figure 3, we show a couple of "typical" events (the first two generated by the computer) for hadron-hadron scattering at $\sqrt{s}$=24 GeV and $p_\perp^{hard}$ = 5 GeV. The figure displays the transverse components of the final parton's momenta plus a picture of the evolution of the event. The first of these events (figure 3a) has in fact an unusually energetic bremstrahlung although the transverse energy is quite typical.

III. TRIGGER BIAS IN LARGE APERTURE CALORIMETERS

In our model hadronic interactions can produce events in which a significant fraction of the produced transverse energy is carried by gluon bremstrahlung, in addition to that carried by the hard-scattering partons. Such events actually occur quite frequently, and lead to a trigger bias effect similar to that observed in small aperture (single particle or jet) triggers. To briefly review the small aperture effect, we recall that attempts to calculate the cross sections for such triggers using lowest order QCD parton interactions and hadronic wave functions without constituent transverse momentum give results which are smaller than the data. The effect has been explained by the introduction of a fixed constituent transverse momentum distribution with an average $p_\perp$ of 850 MeV/c (6). The basic parton interaction feeding a given trigger then takes place from initial states in which the partons are preferentially directed towards the trigger, the Q^2 of their hard scattering is reduced, and the QCD cross section in enhanced. It was also recognized in ref. (6) that the intrinsic transverse momentum distribution is not really fixed, but evolves with Q^2 as in our current model. The evolution results in intrinsic transverse momentum effects which remain important at large $\sqrt{s}$ and large $p_\perp^{hard}$, and to radiated partons accompanying large values of $p_\perp^{brems}$ (t_B^{min}) which are an important feature of the final state. It is these radiated partons which lead to large aperture trigger bias effects. For scattering at a given $p_\perp^{hard}$, although the bulk of the events will appear jetlike with $p_\perp^{obs} \sim p_\perp^{hard}$, fluctuations will produce a "tail" in which $p_\perp^{obs}$ is much larger. If one now concentrates experimentally on a fixed range of $p_\perp^{obs}$ accepted into a large aperture calorimeter, the question is whether the cross section is dominated by

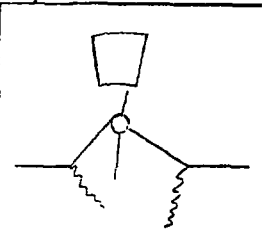

small aperture trigger bias

events with $p_\perp^{hard} \sim p_\perp^{obs}$ or the tail from scattering at smaller $p_\perp^{hard}$. Because the parton-parton cross section (shown in Figure 2) is a steeply falling function of $p_\perp^{hard}$ one expects the tail to be important, and this is our basic mechanism for large aperture trigger bias. The small and large aperture trigger biases come from the same physics, gluon bremstrahlung. For a small aperture trigger the bremstrahlung gluons are opposite the trigger while in the large aperture case the gluons actually enter the trigger calorimeter. A similar effect has been considered by Singer et al. (11), but with a fixed momentum distribution and fragmenting beam and target jets rather than explicit paron bremstrahlung in the initial state. Before describing our calculations in detail we illustrate the magnitude of the effect by giving our results for the SPS fixed target pp experiment NA5 (12). This experiment at $\sqrt{s}$=24 GeV accepts events populating a fiducial region covering 2π in azimuth and $54° < \Theta_{cm} < 135°$ in polar angle, and with accepted E_T up to 18 GeV. (Measurements are also made for smaller azimuthal acceptances, but we do not consider these since they are more sensitive to hadronization). The cross section, $d\sigma/dE_T$ is characterized by a linear exponential behavior of approximately $\exp(E_T)$, and an absolute normalization about an order of magnitude larger than an estimate from a QCD jet model without parton bremstrahlung (but with hadronization). Figure 4 shows the NA5 data along with calculations at parton level from our model and from QCD jet model without bremstrahlung. Our results match the slope of the data, but are smaller by about an order of magnitude. Both hadronization and the unfolding of the experimental E_T resolution (which is ~5% for NA5) would tend to reduce this difference. The use of E_T rather than $\Sigma|p_T|$ to plot the experimental data accentuates the effects of hadronization. We note that the hadronized QCD jet model used by the NA5 group gives cross sections about an order of magnitude larger than our unhadronized version (the open circles in Figure 4). If hadronization effects are of similar magnitude for the full model with bremstrahlung, it will end up being quite close to the data. Aside from such caveats concerning the overall normalization Figure 4 illustrates our main point: already at the parton level gluon radiation effects greatly enhance the QCD jet cross section.

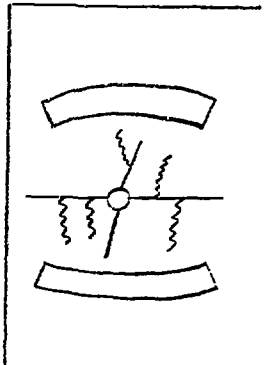

large aperture trigger bias

IV. THE DRELL-YAN PROCESS

The cross section integrated over all $p_\perp$ for the Drell-Yan process $\bar{p}p \to \mu^+\mu^- x$ is essentially identical in our model to that calculated from standard QCD techniques. In particular we would presumably need to renormalize our results up by a factor ~2 to 3 to agree with the experimental measurements (13) however the $p_\perp$ distribution of the lepton pair is not calculable from the standard techniques and this allows both significant tests of our model and an opportunity to optimize our parameters. The application of our model to this case has already been described in Ref 2. Here we note that our formalism is in this case more precise formulation of the pioneering work of Parisi and Petrorzio (14). The leading logarithm approximation used in our model has the advantage that it can be summed to all orders but the severe disadvantage of not even being exact to $O(\alpha_s)$. As shown in Ref. 2 for the application to e^+e^- annihilation, one can modify the model to retain the all orders summation but reduce to the exact $O(\alpha_s)$ (or even $O(\alpha_s^2)$) QCD calculations. Unfortunately we have yet to put this improvement into the Drell-Yan calculation and so our results in this case are still preliminary. However they are still quite satisfactory for determining a resonable set of parameters with which to study hadron-hadron scattering. Thus the latter has quite different $O(\alpha_s)$ terms to the Drell-Yan case and so one would have to improve both calculations (by adding in the exact low order calculations) to be consistent. Although this ambitious program is possible for the Drell-Yan calculation, there are substantial technical difficulties for the hadron-hadron scattering application (10). In this paper, we will treat all processes with the universal leading logarithm approximation for the bremstrahlung.

In Figure 5, we plot the longitudinal momentum dependence of the mean transverse momentum appropriate for a Drell-Yan mass of 5.5 GeV at a $\sqrt{s}$ of 27.4 GeV. This figure illustrates two important points. Firstly note that the gluons have substantially larger $\langle p_\perp^{brem}\rangle$ than the quarks or anti-quarks. This follows from the larger $G \to GG$ than $q \to q\,G$ coupling in QCD. The difference between quarks and gluons persists to higher energies. For instance one finds on integrating over lognitudinal momentum that

at $\sqrt{s}$ = 62 GeV, m = 15 GeV: $\langle p^{brem}|quark\rangle = 1.1$ GeV
$\langle p^{brem}|gluon\rangle = 1.8$ GeV

at $\sqrt{s}$ = 540 GeV, m = 80 GeV: $\langle p^{brem}|quark\rangle = 2.9$ GeV
$\langle p^{brem}|gluon\rangle = 4.4$ GeV

at $\sqrt{s}$ = 2000 GeV, m = 80 GeV: $\langle p^{brem}|quark\rangle = 5.3$ GeV
$\langle p^{brem}|gluon\rangle = 7.2$ GeV

Returning to Figure 5, we also see that $\langle p_\perp^{brem}\rangle$ decreases as the longitudinal fraction x increases. This is also easy to understand because partons at low x are more likely to come from a bremstrahlung than those at large x which are preferentially partons which did not radiate. This effect follows from the necessity that any bremstrahlung will decrease the longitudinal momentum combined with the rapidly decreasing (as x→1) input x distributions.† Note from figure 5, that we have chosen the input $p_\perp^{intrinsic}$ or $p_\perp^{brem}$ (t_B^0 = -4 Gev^2) to have a gaussian distribution with a mean of 750 MeV. (This is 50% larger than the choice in Ref. 2).†† We have chosen $\langle p_\perp^{intrinsic}\rangle$ to be independent of x and parton type. This is not very reasonable because if we had made the same assumption at a lower $t_B^0 \sim -\Lambda^2$, evolution to our choice t_B^0 = -4 GeV^2, would lead to a $\langle p^{brem}$ (-4 GeV^2)$\rangle$ that is larger for gluons than quarks and decreases as x increases. The Drell-Yan data would prefer a modest x dependence in the $\langle p_\perp^{intrinsic}\rangle$ for quarks but there is no quantitative handle (as yet) for the gluons. We have explored choosing lower t_B^0 but have not found very satisfactory results i.e. the fits to the Drell-Yan data seem worse. This is not very surprising because it is neither unreasonable to use leading order perturbative QCD below 4 GeV^2. In any case we will stick with t_B^0 = -4 GeV^2 and a type and x independent $\langle p_\perp^{intrinsic}\rangle$.

In figures 6 to 9, we compare our model with some of the available data on both $\langle p_\perp\rangle$ and the p distributions for pp → $\mu^+\mu^-$x. The agreement is quite good although the model does tend to underestimate the yield at large $p_\perp$. In figure 9 we show that an exact $O(\alpha_s)$ calculation + (19) is slightly better although it too lies below the trend of the data for $\langle p_\perp\rangle$ at $\sqrt{s}$=62 GeV. Note the exact $O(\alpha_s)$ calculation needs a slightly lower $\langle p_\perp^{intrinsic}\rangle$; namely 600 MeV which again indicates that leading log Monto Carlo is under estimating the high p bremstrahlung. In fact, Ref. 18 decomposes the $O(\alpha_s)$ calculation at $\sqrt{s}$=62 GeV, 5<m($\mu^+\mu^-$)<8 GeV into the Compton ($qg\to q\gamma^*$) and annihilation terms ($q\bar{q}\to g\gamma^*$).

†At higher momenta the $\langle p_\perp^{brem}\rangle$ is no longer peaked at x = 0 but rather at an intermediate x value. Now all partons come from bremstrahlung and those at low x are kinematically required to have lower $p_\perp$.

††We have also chosen the upper limit $t_B^{min} = m^2_{\mu^+\mu^-}$ rather than $-m^2_{\mu^+\mu^-}$ as in Ref. 4.

+With a prescription to cutoff the low $p_\perp$ divergence.

The total leading log calculation follows the $O(\alpha_s)$ annihilation term quite closely whereas in the $O(\alpha_s)$ calculation it is the Compton term that dominates at large $p_\perp$. This suggests that the leading log approximation is underestimating the Compton contribution.

V. THE NA5 EXPERIMENT (12)

The mechanism behind the enhancement of the QCD cross sections shown in Figure 4 has been described in Sec. III. Here we wish to examine the effect in more detail by displaying $p_\perp^{hard}$ cross-section spectra and the shape properties of biased events. In Figure 10 we show $d\sigma/dp_\perp^{hard}$ for scattering into two fixed $p_\perp^{obs}$ ranges at NA5. The area under the curves corresponds to the observed cross section. For comparison, we show both the contributions from a fully evolved calculation and from a calculation with no parton branching. The unevolved calculation is peaked at $p_\perp^{hard} \sim p_\perp^{obs}$, while the evolved calculation has a tail extending to low values of $p_\perp^{hard}$ and as a result has an order of magnitude larger integrated cross section. When integrating over $p_\perp^{hard}$ we impose a lower limit of 2 GeV to avoid low values where our perturbative calculations become particularly ambiguous. Figure 10 indicates that this low $p_\perp^{hard}$ region may give a significant (but essentially unknown) contribution for $p_\perp^{obs} \lesssim$ 4-5 GeV/c, and in this region the cross sections in Figure 4 may be understimated. An overall view of the $p_\perp^{hard}$ spectrum is given in Figure 11 where the $p_\perp^{obs}$ distributions from fully evolved calculations are plotted for various values of $p_\perp^{hard}$. Each distribution is peaked near $p_\perp^{obs} \approx p_\perp^{hard}$, but in integrating over $p_\perp^{hard}$ at a fixed value of $p_\perp^{obs}$ one sees that the contribution of each peak will be accompanied by a larger contribution from the tails of distributions with $p_\perp^{hard} < p_\perp^{obs}$.

Choosing events with $p_\perp^{hard} < p_\perp^{obs}$ produces clear trigger bias in the form of high parton multiplicity and a generally non-jet-like character of the final states. This is seen in Figure 12 which displays events with $p_\perp^{obs}$ = 5 GeV/c and $p_\perp^{hard}$ = 3 and 3.5 GeV/c. Again we show the first two events generated by the computer which satisfy the given conditions. These events should be compared with the unbiased events in Figure 3.

The same effect can be seen statistically in planarity distributions. The planarity is P=(a-b)/(a+b), where a (b) is the sum of squares of projected momenta along the major (minor) axis of the

transverse momentum tensor. Jet-like events characterized by values of P near one, and round events by P near zero. In Figure 13 we show the planarity distributions from NA5 for events with several $p_\perp^{obs}$ thresholds along with calculated distributions for a low $p_\perp$ cluster model and a QCD jet model with hadronization. In Figure 14 we show planarity distributions from our calculation at several values of $p_\perp^{hard}$ and a $p_\perp^{obs}$ threshold of 5 GeV/c. As expected the planarity distributions become broader and less peaked towards P=1 as $p_\perp^{hard}$ decreases below $p_\perp^{obs}$. One should be careful in comparing Figures 13 and 14 because planarity is a quadratic quantity, similar to sphericity, and is very sensitive to hadronization. For example, the QCD-jet distribution in Figure 13 comes from a model that gives a δ-function at P=1 at parton level. Thus, although the integral over $p_\perp^{hard}$ of the distributions in Figure 14 will contain a broad high-P enhancement, this will be substantially degraded by hadronization.

VI. EARLY RESULTS FROM UA1

As a final illustration of our results we show calculations and data for the transverse energy distribution of the SPS collider experiment UA1 (20). This is shown in Figure 15 where the calculated points are normalized to a total inelastic $\bar{p}p$ cross section of 50 mb at $\sqrt{s}$ = 540 GeV. Here our parton level calculations do not do nearly as well as they did for NA5. A feature of the UA1 data is that even for the very large transverse energies observed, all events seem to be made up of numerous soft particles with an average E_T per particle of about 500 MeV. This indicates the presence of large hadronization effects. Our calculations also indicate this; they produce events with high parton multiplicities and very non-jetlike shapes. Work is in progress to include hadronization in our calculations, and to make quantitative comparisons with both the NA5 and the SPS collider data. Two typical events are shown in Figure 16.

We thank the UA1 group for permission to use their data in Figure 15, but at the experimentors request we also warn the reader that these data are very preliminary.

REFERENCES

(1) G. Altarelli and G. Parisi, Nucl. Phys. B126, 298 (1977).

(2) G.C. Fox, Lectures presented at the 1981 SLAC Summer School, CALT-68-863, 1981.

(3) R. Odorico, paper presented at the Forward Collider Workshop, Madison (1981).

(4) G.C. Fox and S. Wolfram, Nucl. Phys. B168, 285 (1980).

(5) R. Odorico, Nucl. Phys. B172, 157 (1980). P. Mazzanti and R. Odorico, Phys. Lett. 95B, 133 (1980) and Z. Physik C7, 61 (1980).

(6) R.P. Feynman, R.D. Field and G.C. Fox, Phys. Rev. D18, 3320 1978).

(7) R.P. Feynman and R.D. Field, Nucl. Phys. B136, 1 (1978).

(8) C. Bromberg et al., Nucl. Phys. B171, 1 (1980).

(9) W.E. Caswell, R.R. Horgan and S.J. Brodsky, Phys. Rev. D18, 2415 (1978).

(10) R.K. Ellis, M.A. Furman, H.E. Haber and I. Hinchliffe, Nucl. Phys. B173, 397 (1980).

(11) R. Singer et al., ANL-HEP-PR-81-25, 1981.

(12) K. Pretzl, paper presented at the Forward Collider Workshop, Madison (1981).

(13) R. Stroynowski, Physics Reports 71, 1 (1981).

(14) G. Parisi and R. Petronzio, Nucl. Phys. B154, 427 (1979).

(15) D.M. Kaplan et al., Phys. Rev. Letters 40, 435 (1977)

(16) J.K. Yoh et al., Phys. Rev. Letters 41, 684 (1978).

(17) D. Anbreasyan et al., "Production Mechanisms of High Mass Muon Pairs", preprint (1981).

(18) D. Anbreasyan et al., "Dimuon Scaling Comparison at 44 and 62 GeV", MIT technical report 119 (1981).

(19) R.D. Field, "Perturbative Quantum Chromodynamics and Applications to Large Momentum Transfer Processes", CALT-68-739 and La Jolla Summer School Notes, (1979).

(20) A. Kernan, paper presented at the Forward Collider Workshop, Madison (1981).

ACKNOWLEDGMENT

This work was supported by the Division of High Energy Physics of the U.S. Department of Energy under Contract Nos. W-7405-ENG-48, and DE-AC03-81-ER40050.

Table 1. Notation for Virtual Masses

		where defined			
		initial state evolution	hard scatter	final state evolution	hadronization
t	Virtual m^2 of current parton during evolution	during		during	
t_B^0	Initial m^2 that starts initial state evolution $t_B^0 = -4\ \mathrm{GeV}^2$	before			
t_B^{min}	Lower limit on (negative) virtual m^2 for partons in final state evolution $t_B^{min} = -4m^2$ for Drell Yan $t_B^{min} = -4\ p_{hard}^2$ for hadron hadron scattering	after	before		
t_B^{max}	Upper limit of (positive) virtual m^2 for partons in final state evolution. $t_B^{max} = -t_B^{min}$ for partons just after hard scatter. t_B^{max} for bremstrahlung partons depends on exact kinematics (eq. (5.10) of Ref. 2)		after	before	
t_A^{min}	Lower limit on (positive) virtual m^2 for partons in final state. $t_A^{min} = 10\ \mathrm{GeV}^2$.			after	before

Table II. Notation for transverse momenta

		where defined: initial state evolution	hard scatter	final state evolution	hadronization
$p_\perp^{intr} = p_\perp^{brem}(t_B^0)$	The intrinsic $p_\perp$ distribution at the initial mass scale $t = t_B^0$	before			
$p_\perp^{brem}(t_B^{min})$ $t \geq t_B^{min}$	The $p_\perp$ distribution generated from $p_\perp^{intr}$ and the evolution for partons of (negative) $t \geq t_B^{min}$. This is universal in Drell Yan, hadron hadron, NN scattering etc.	after	before		
$p_\perp^{hard}$	The $p_\perp$ induced by the hard two body collision for hadron-hadron scattering $p_\perp^{hard} = 1/2\sqrt{-t_B^{min}}$	after	at	before	
$p_\perp^{obs} = \frac{1}{2}\sum\lvert p_\perp\rvert$	The observed transverse momentum (which is equal to $E_T/2$ at the parton level).				after

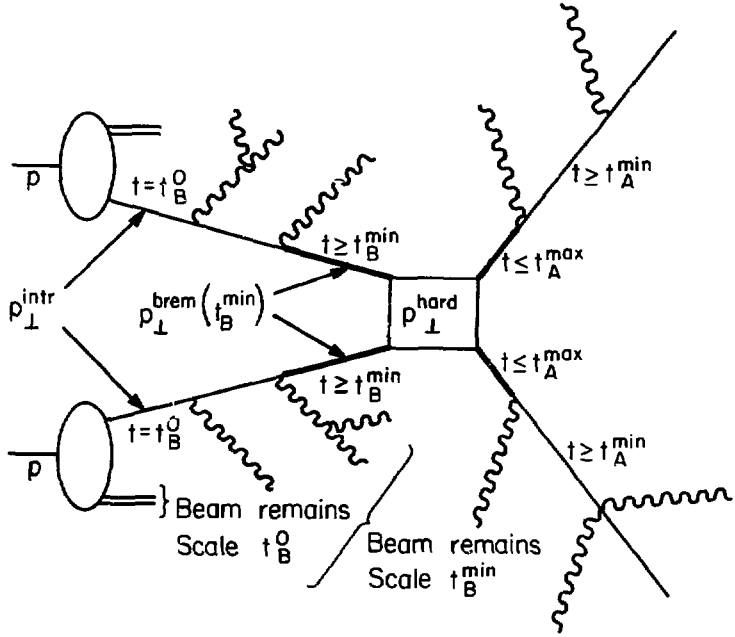

Fig. 1: The picture of hadron hadron scattering used in this paper and described in Section II. The notation is defined in Tables 1 and 2.

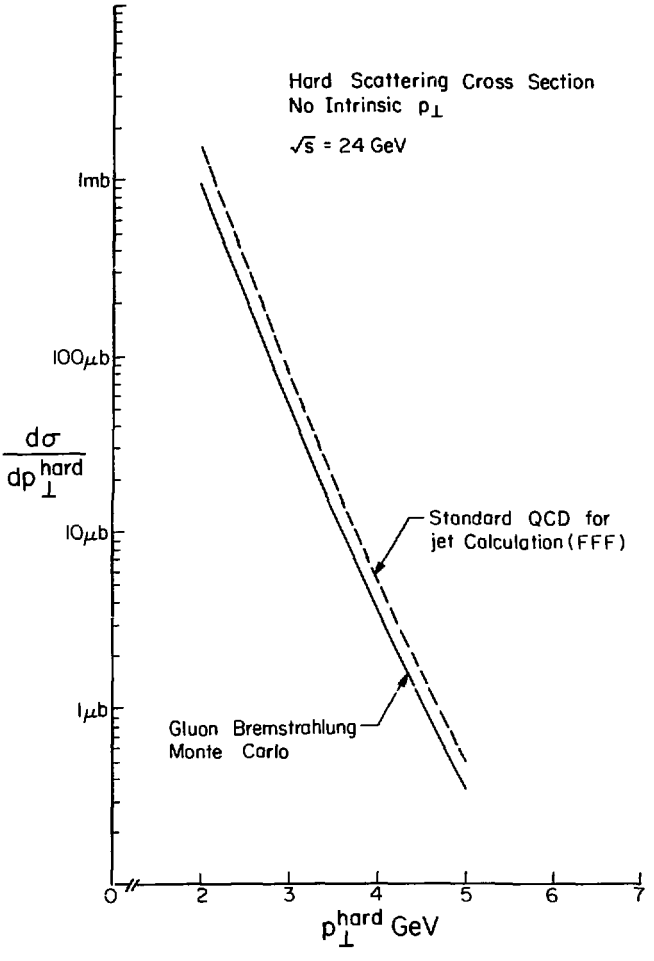

Fig. 2: Comparison of the hard scattering cross section from a conventional QCD calculation (Ref. [6], dashed line) with that from the techniques used in this paper (solid line). The differences are discussed in Section II.

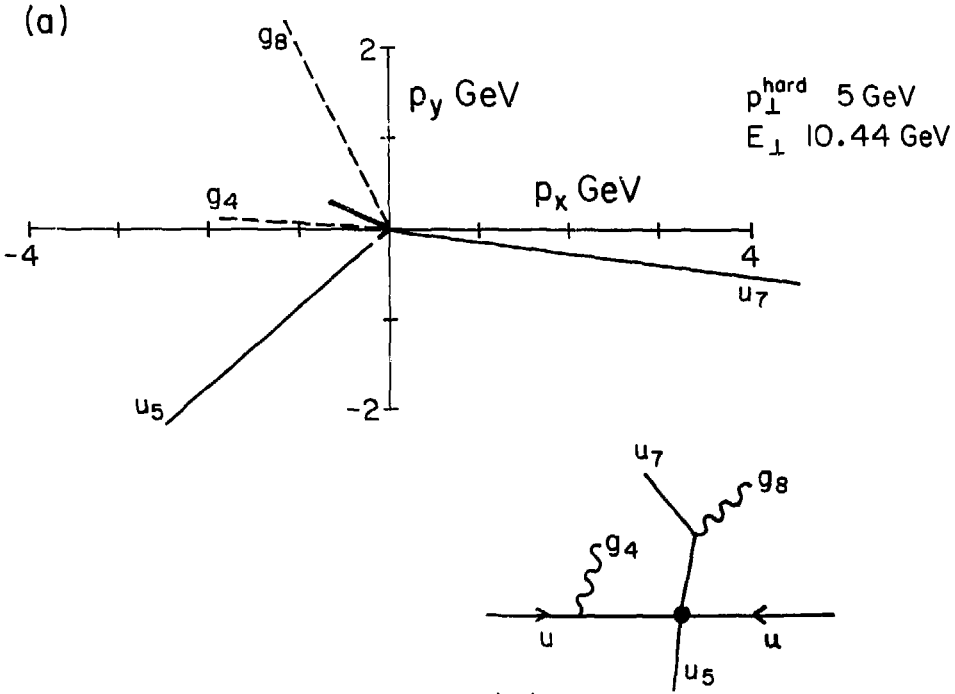

Fig. 3(a): Unbiased events for $\sqrt{s}$ = 24 GeV and $p_\perp^{hard}$ = 5 GeV. The top part of the diagram shows the structure of the final state in the transverse (p_x, p_y) plane. Dashed lines are gluons, solid lines (anti)quarks and (two) thick lines denote the beam remains. The event is displayed so that the x direction is along the major axis of a planarity analysis (Section V). Below this diagram we show the evolution of the event as a Feynman diagram. The solid circle represents the hard (2 → 2) scatter. The remaining vertices are bremstrahlung.

(b)

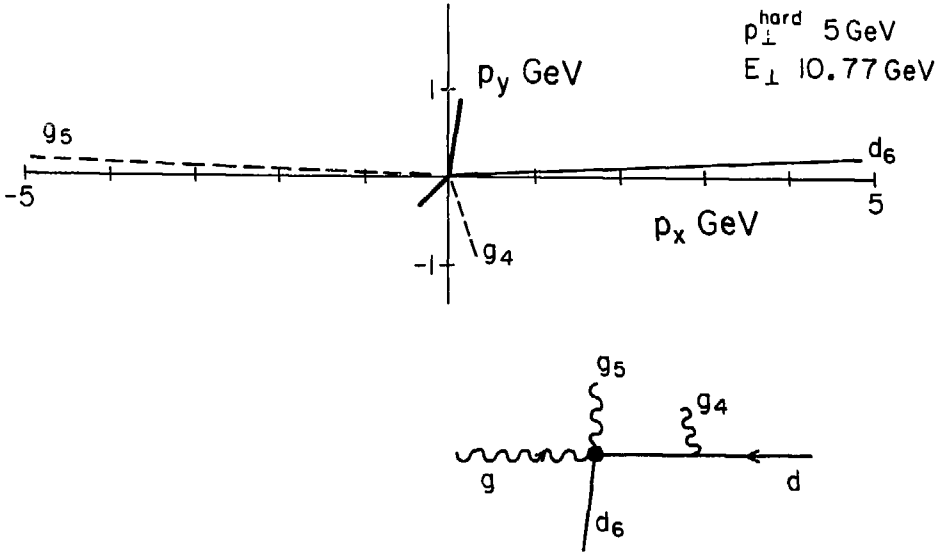

Fig. 3(b): Unbiased event for $\sqrt{s}$ = 24 GeV and $p_\perp^{hard}$ = 5 GeV. The notation is the same as in Fig. 3(a).

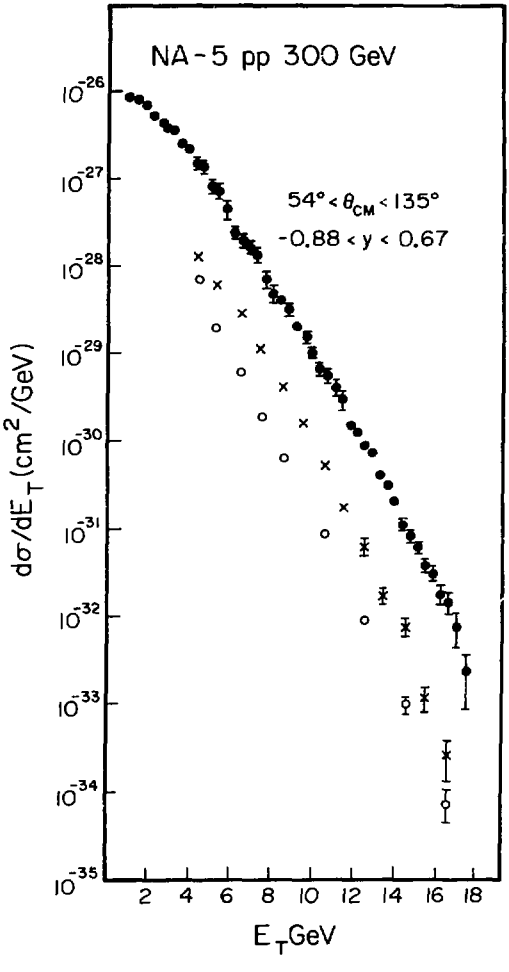

Fig. 4: Comparison of NA5 cross section data (●) and parton level calculations with (x) and without (O) bremstrahlung.

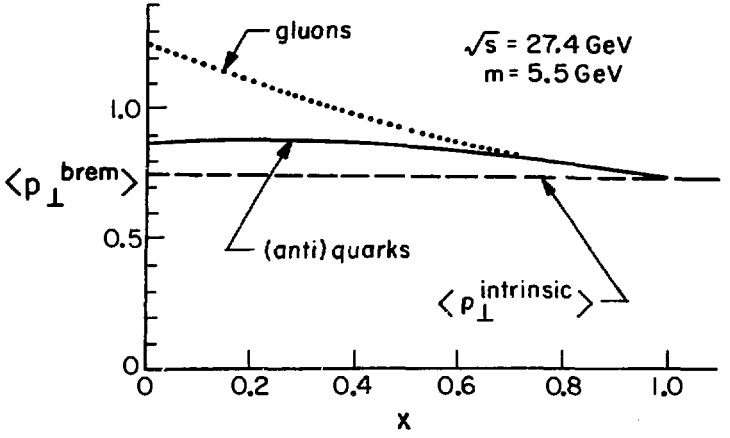

Fig. 5: Longitudinal (x) dependence of $\langle p_\perp^{brem} \rangle$ appropriate for Drell-Yan scattering at $\sqrt{s}$ = 27.4 GeV and a mass of 5.5 GeV.

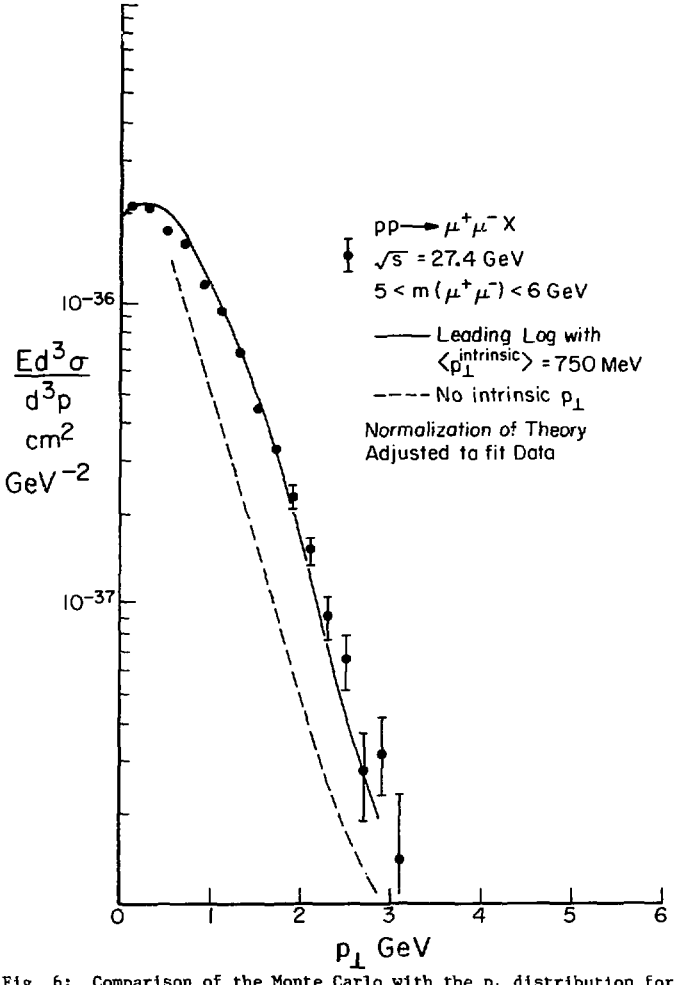

Fig. 6: Comparison of the Monte Carlo with the $p_\perp$ distribution for the Drell-Yan μ pairs at $\sqrt{s}$ = 27.4 GeV and a mass of 5.5 GeV [Ref. 15]. The normalization of the theory has been adjusted to fit the data while we show separately the calculation that ignores the intrinsic $p_\perp$ of 750 MeV.

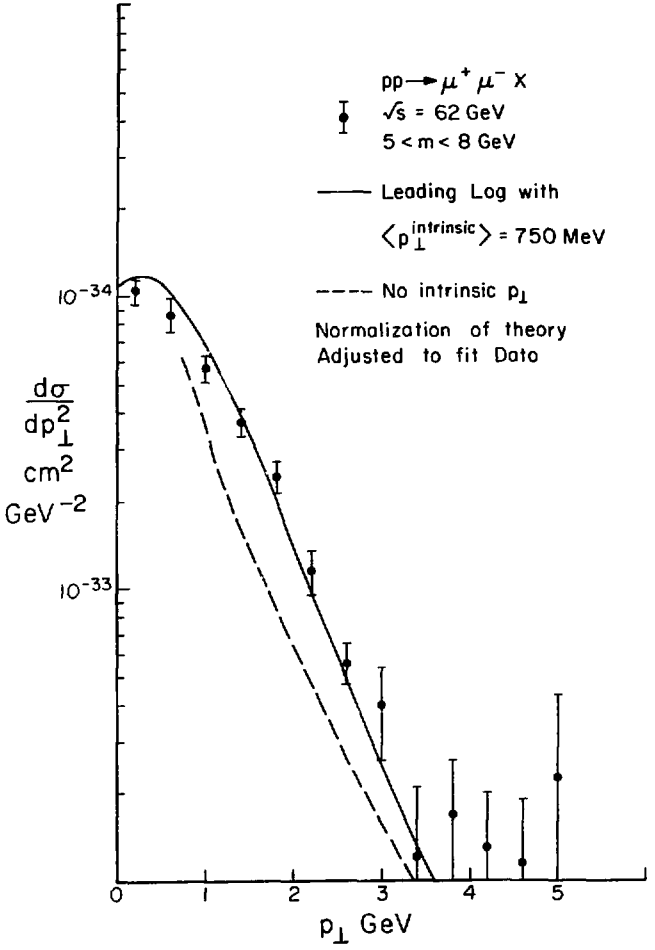

Fig. 7: As Fig. 6 but the data from Ref. 18 has $\sqrt{s}$ = 62 GeV and corresponds to the mass range of 5 to 8 GeV.

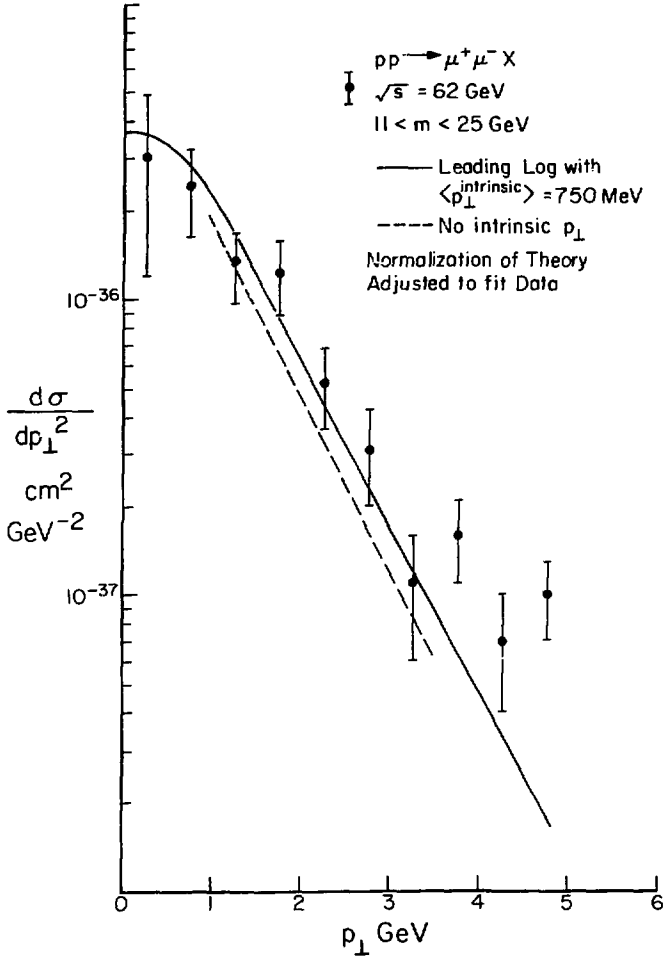

Fig. 8: As Fig. 6 but the data from Ref. 17 have $\sqrt{s}$ = 62 GeV and correspond to the mass range of 11 to 25 GeV.

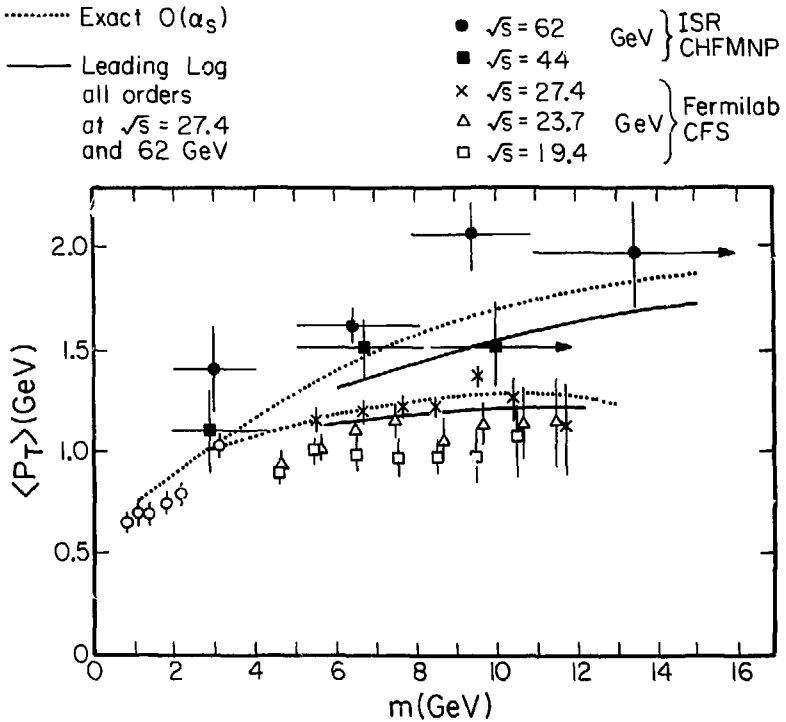

Fig. 9: The mass dependence of the $\langle p_\perp \rangle$ of the Drell-Yan μ pairs from the data of Ref. 16 ($\sqrt{s}$ = 19.4, 23.7 and 27.4 GeV) and Ref. 17 ($\sqrt{s}$ = 44 and 62 GeV). The leading log Monte Carlo calculations are shown at $\sqrt{s}$ = 27.4 and 62 GeV as a solid curve. The exact $O(\alpha_s)$ calculation of Ref. 19 at the same energies is shown as a dotted line. This figure is adapted from one in Ref. 17.

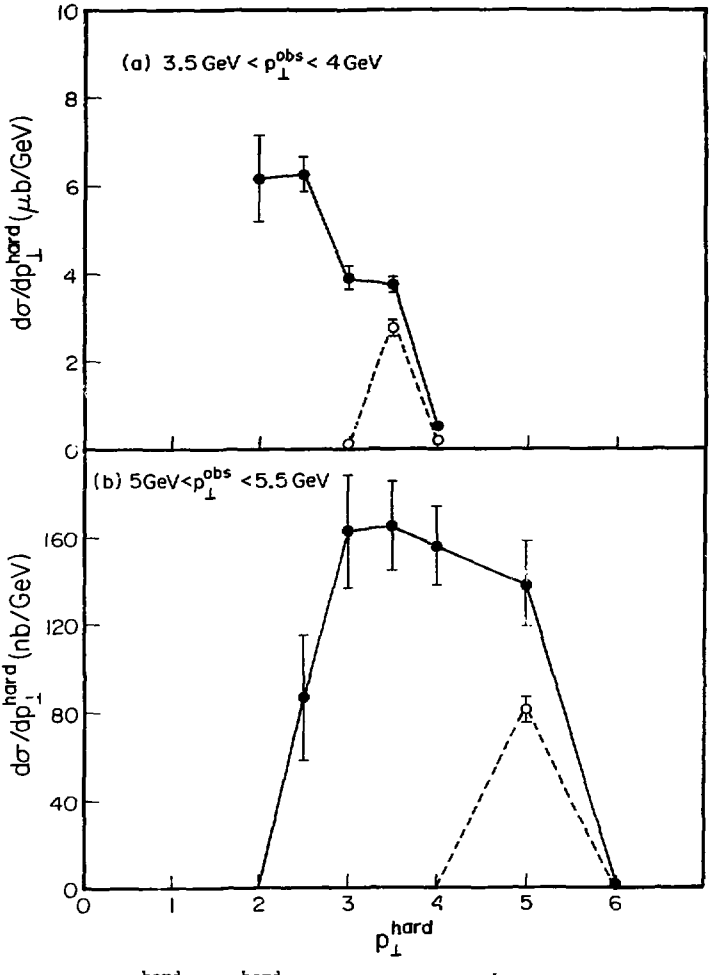

Fig. 10: $d\sigma/dp_\perp^{hard}$ vs. $p_\perp^{hard}$ for two ranges of $p_\perp^{obs}$ at the NA5 calorimeter, calculated with (●) and without (O) bremstrahlung. The area under the curves corresponds to the observable cross section within the given $p_\perp^{obs}$ ranges.

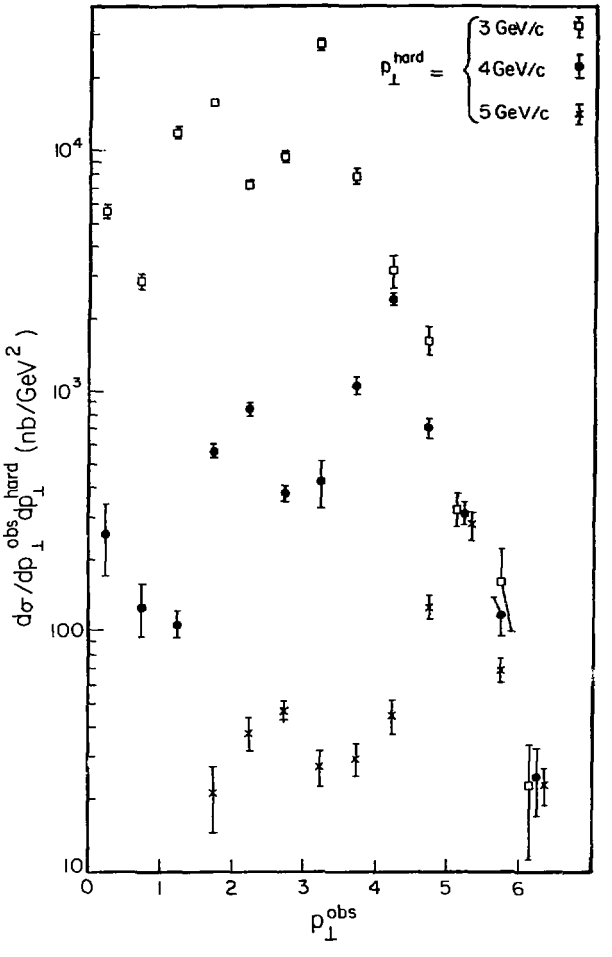

Fig. 11: $d\sigma/dp_\perp^{hard}\, dp_\perp^{obs}$ at the NA5 calorimeter calculated for three values of $p_\perp^{hard}$.

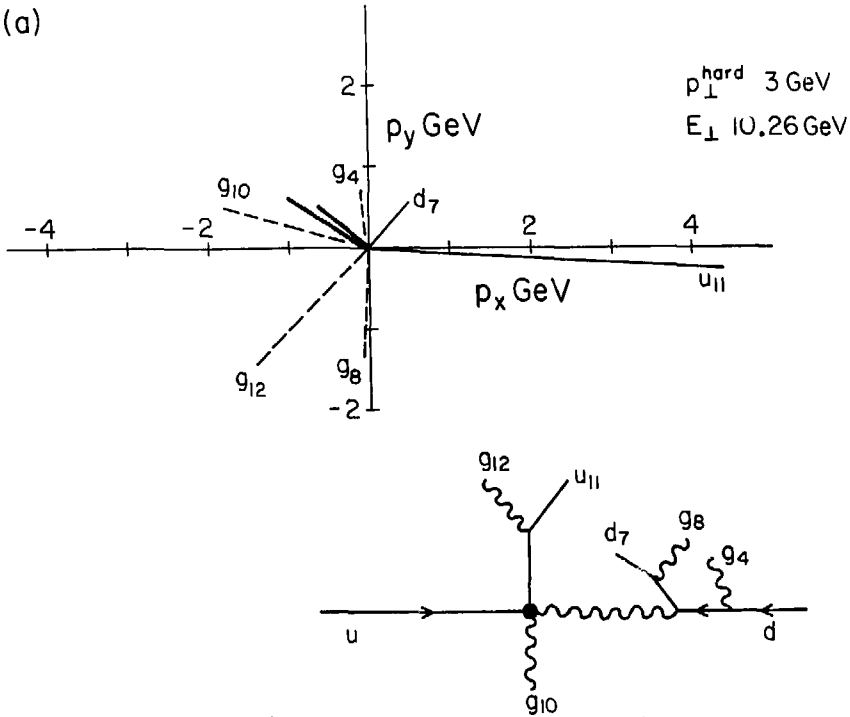

Fig. 12(a): Biased event satisfying $2p_\perp^{obs} = E_\perp = 10$ GeV at $\sqrt{s} = 24$ GeV and $p_\perp^{hard}$ of 3 GeV. The top part of the diagram shows the structure of the final state in the transverse (p_x, p_y) plane. Dashed lines are gluons, solid lines (anti)quarks and (two) thick lines denote the beam remains. The event is displayed so that the x direction is along the major axis of a planarity analysis (Section V). Below this diagram we show the evolution of the event as a Feynman diagram. The solid circle represents the hard (2 → 2) scatter. The remaining vertices are bremstrahlung.

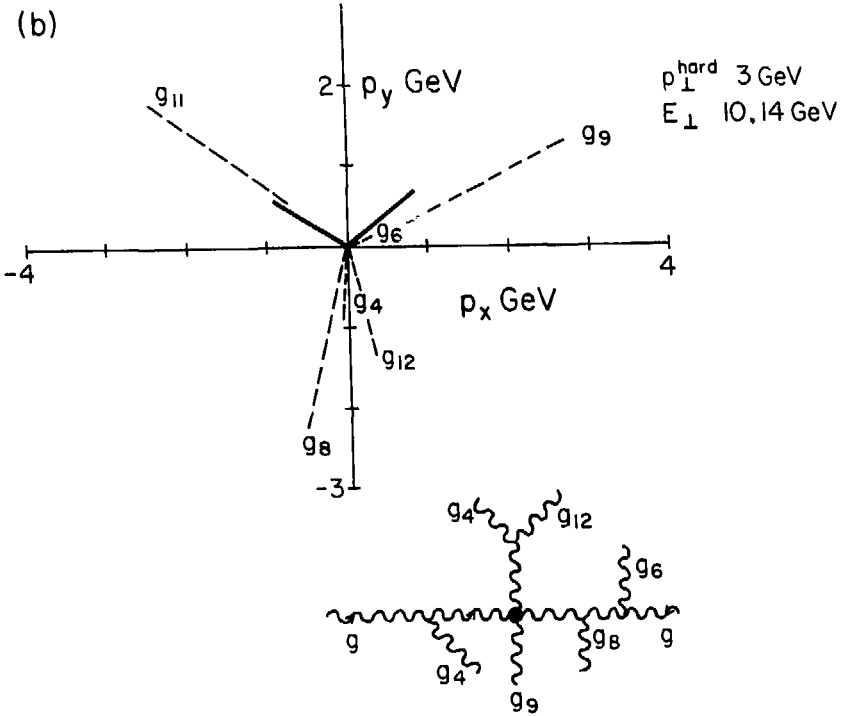

Fig. 12(b): Biased event satisfying $2p_\perp^{obs} = E_\perp > 10$ GeV at $\sqrt{s} = 24$ GeV and $p_\perp^{hard}$ of 3 GeV. The notation is described in the caption to Fig. 12(a).

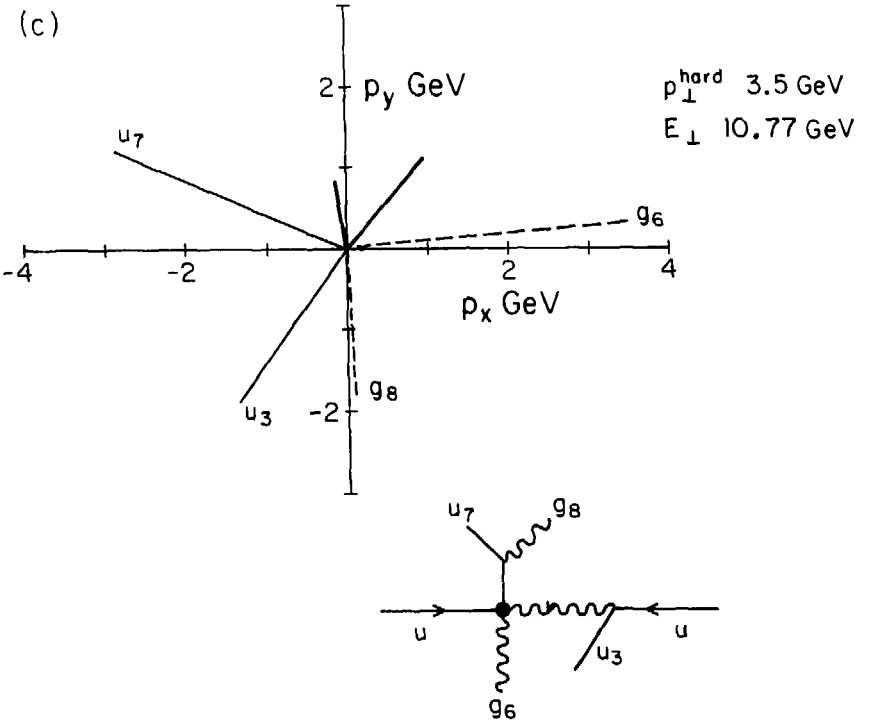

Fig. 12(c): Biased event satisfying $2p_\perp^{obs} = E_\perp = 10$ GeV at $\sqrt{s} = 24$ GeV and $p_\perp^{hard}$ of 3.5 GeV. The notation is described in the caption to Fig. 12(a).

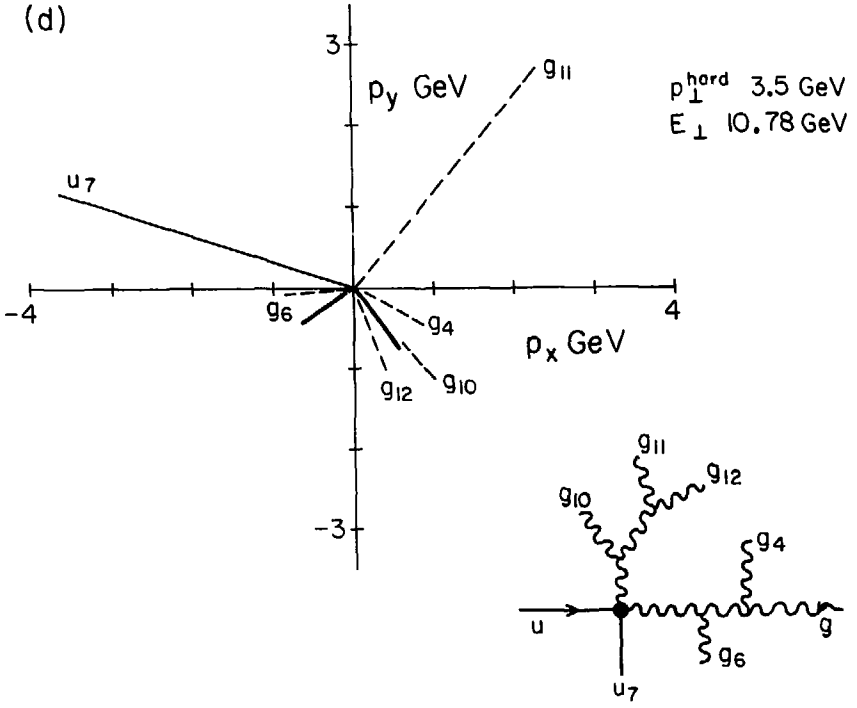

Fig. 12(d): Biased event satisfying $2p_\perp^{obs} = E_\perp > 10$ GeV at $\sqrt{s} = 24$ GeV and $p_\perp^{hard}$ of 3.5 GeV. The notation is described in the caption to Fig. 12(a).

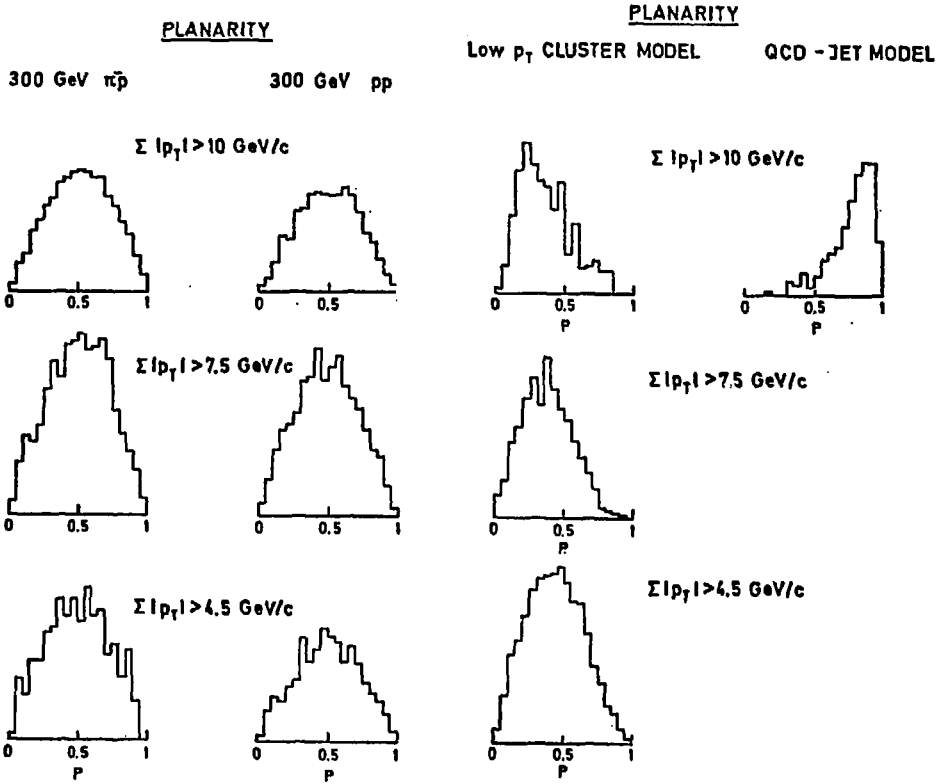

Fig. 13: Planarity distributions of events selected by the NA5 calorimeter trigger from π^-p and pp collisions at 300 GeV/c for different trigger thresholds. Results from a low $p_\perp$ cluster model and a QCD-4 jet model are shown for comparison.

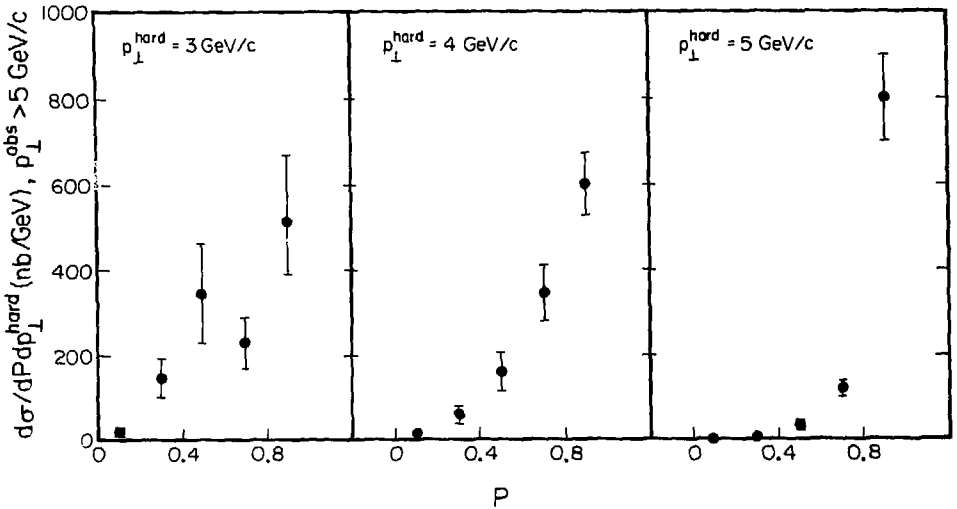

Fig. 14: Planarity distributions at the NA5 calorimeter for three values of $p_\perp^{hard}$.

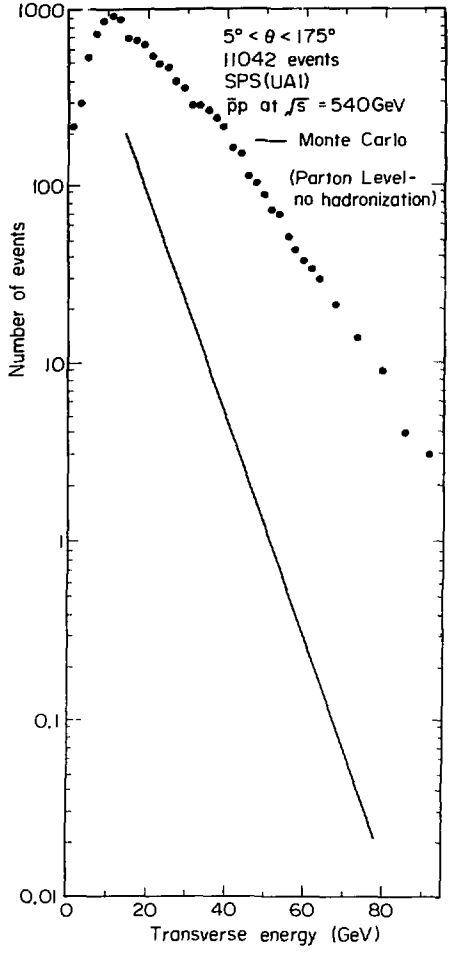

Fig. 15: Data and parton level calculations of the UA1 $\bar{p}p$ transverse energy distribution at $\sqrt{s}$ = 540 GeV.

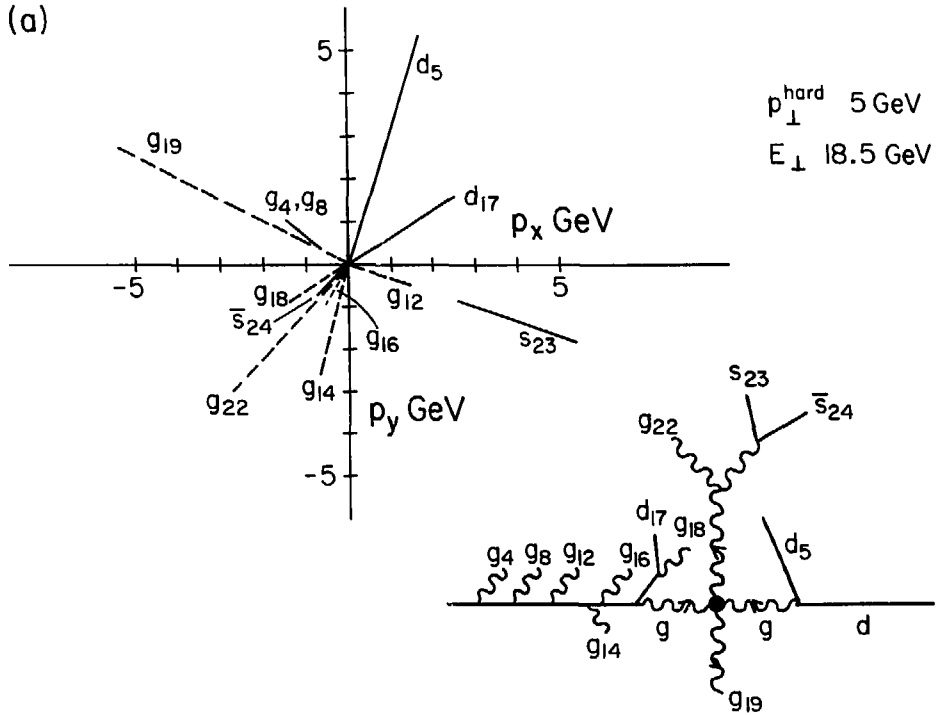

Fig. 16(a): Biased event satisfying $2p_\perp^{obs} = E_\perp > 18$ GeV at $\sqrt{s} = 540$ GeV and $p_\perp^{hard} = 5$ GeV. The notation is described in the caption to Fig. 12(a).

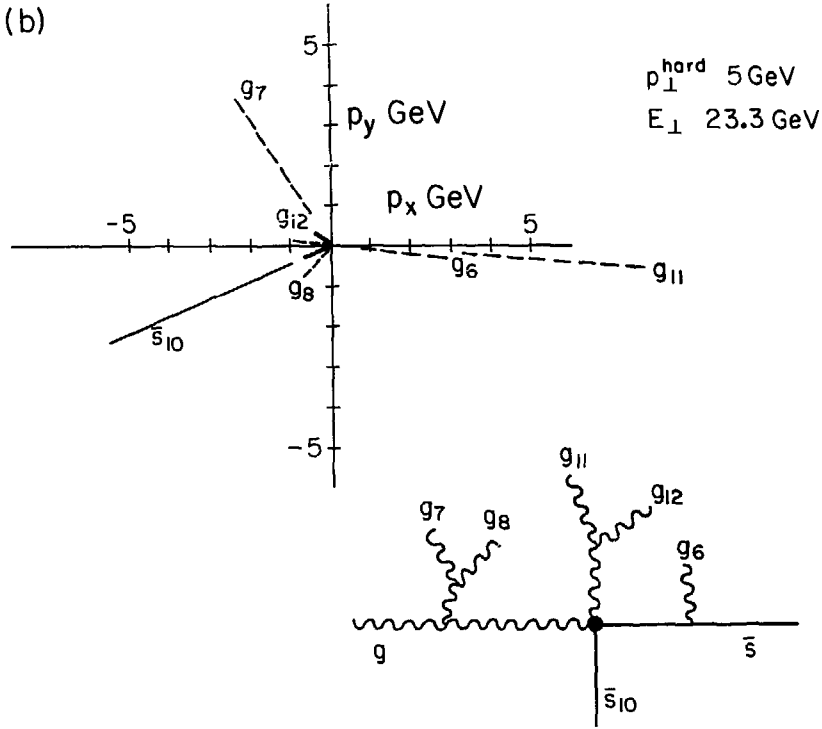

Fig. 16(b): Biased event satisfying $2p_\perp^{obs} = E_\perp \simeq 18$ GeV at $\sqrt{s} = 540$ GeV and $p_\perp^{hard} = 5$ GeV. The notation is described in the caption to Fig. 12(a).